State Key Laboratory of Metastable Materials Science and Technology[1], Yanshan University, Qinhuangdao, Institute of Applied Chemistry[2], Hebei North University, Zhangjiakou; Drug Support Center[3], Peoples Liberation Army General Hospital, Beijing, China

A composite of graphene oxide and iron oxide nanoparticles for targeted drug delivery of temozolomide

Li-Hua Wang[1,2], Lin Sui[3], Peng-Hui Zhao[2], Hai-Di Ma[2], Jia-Yuan Liu[2], Zhen Wei[2,*], Zai-Ji Zhan[1], Yong-Li Wang[2]

Received October 21, 2019, accepted January 17, 2020

**Corresponding author: Zhen Wei, No. 11, Zuanshinan Road, Zhangjiakou, Hebei 075000, China zjzhan@ysu.edu.cn*

Pharmazie 75: 313-317 (2020) *doi: 10.1691/ph.2020.9170*

A magnetic targeting nanoparticle based on graphene oxide-ferroferric oxide (GO-Fe_3O_4) was investigated as a potential drug delivery vehicle. The formation of GO/Fe_3O_4 hybrid material was confirmed by Fourier transform infrared spectroscopy, X-ray diffraction, scanning electron microscopy and transmission electron microscopy. The GO/Fe_3O_4 hybrid still shows a higher saturation magnetization of 58.42 emu/g after coating with graphene oxide. Drug loading and releasing experiments demonstrate the GO-Fe_3O_4 hybrid has a good loading capacity of (6.47±0.08) mg/mg for temozolomide and a satisfactory release under slightly acidic condition. The MTT assays of glioma C6 cells exhibits the GO-Fe_3O_4 hybrid does not display toxicity with the concentration ranged from 40 to 120 μg/mL *in vitro*, while the complex of temozolomide loaded on GO/Fe_3O_4 has a better inhibitory effect on the proliferation of rat glioma C6 cells. All results suggest the prepared GO/Fe_3O_4 has potential applications in targeted anticancer drug delivery.

1. Introduction

With the development of modern industrialization, nanoscale drug carriers have emerged as a bridge linking nanotechnology and drug delivery, involving liposomes, microspheres (Deng et al. 2005), nanoparticles (Pankhurst et al. 2003) and polymeric shells (Noble et al. 2004; Bédard et al. 2008). The medicine is loaded on these nanoscale carriers, which have the characteristics of targeting, improve solubility and bioavailability. However, the loading capacity of the current nanoscale drug carrier is still low. Therefore, developing an efficient drug carrier is critical in drug carrier research.

Recently, graphene oxide (GO) has attracted great attention due to its large specific surface area for efficient drug binding and abundant functional groups (such as -OH, -COOH, -O-, -C = O, etc.) for improving solubility (Yang et al. 2016; Wang et al. 2011). As a drug carrier, GO and drugs could form complexes through π-π conjugated, hydrogen bonding or an ionic reaction. Moreover, GO derivatives are reported to have significantly improved tumor passive targeting effect and higher tumor uptake *via* the enhanced permeability and retention effect (Pramanik et al. 2019). Magnetic nanoparticles can be manipulated by an external magnetic field and play a targeting role (Guo et al. 2016; Li et al. 2018). As one of the magnetic substances, Fe_3O_4 is widely used in biomedical applications such as drug delivery, magnetic resonance imaging, magnetic hyperthermia, and cell labeling and separation (Cole et al. 2011; Schleich et al. 2014). Combining the characteristics of GO and Fe_3O_4, the magnetic GO/Fe_3O_4 carrier has the ability of passive targeting, and can be located at the designated site and release the drugs under the magnetic field *in vitro*. Furthermore, cell viability and metabolic activity decrease significantly when cells are exposed to high iron oxide nanoparticle concentrations.

Temozolomide (TMZ), a novel small molecule alkylating agent with activity in the central nervous system, is able to pass the blood-brain barrier (Prabhu et al. 2017; Nordling-David et al. 2017). Despite its important role in chemotherapy for glioblastoma treatment, the cytotoxicity and bioavailability of TMZ to normal cells cannot be ignored. Besides, due to its short half-life, the concentration of TMZ around the brain rarely reaches therapeutic levels. To improve its application, a lot of experimental work has been reported in the literature. However, low drug loading capacity still limited the use of TMZ.

In the context of the current studies for magnetic nanoparticles, the aim of this work is to synthesize a GO-Fe_3O_4 nanoparticles hybrid by chemical deposition method and investigate the binding of TMZ on the hybrid. The morphology, microstructure and magnetic properties were examined by transmission electron microscopy (TEM), scanning electron microscopy (SEM), Fourier transform infrared spectrometer (FT-IR) and X-ray diffractometer (XRD), respectively. The loading and release behavior of TMZ was also evaluated. The results demonstrated that the Fe_3O_4/GO composites have high loading capacity, favorable magnetism and low cytotoxicity, which is helpful to conduct the further study of loading and releasing drugs.

2. Investigations, results and discussion

2.1. Synthesis and characterization of samples

The SEM and TEM images of GO and GO-Fe_3O_4 at different magnifications were shown in Figs. 1 and 2, respectively. It can be seen that GO showed two- dimensional structure, similar to graphene, which was consistent with previous reports (Li et al. 2012). Different from GO, the structure of GO in GO-Fe_3O_4 was distorted (Figs. 1C and 1D), the uniform Fe_3O_4 particles were distributed randomly on the surface or edges of GO (Figs. 2C and 2D). The particle diameters of GO and GO-Fe_3O_4 measured by dynamic light scattering were 202.4±15.1 and 239.8±17.4 nm, respectively. And the nanocomposites dispersed in water showed negative zeta potential values of 34.2±3.2 mV (GO) and 38.7±4.1 mV (GO-Fe_3O_4). The enlarged particle size and zeta potential could be attributed to chemical impurities retained in GO (Yue et al. 2012). Some scholars suggested that it may be related to higher drug loading capacity (Chai et al. 2017).

The crystal phases of GO and GO-Fe_3O_4 were analyzed by X-Ray Diffraction (XRD). As presented in Fig. 3(a), the diffraction peak of GO appeared at 11.8° (001). Six diffraction peaks of GO-Fe_3O_4 appeared at 31.5° (220), 36.47° (311), 44.09° (400), 53.87° (422),

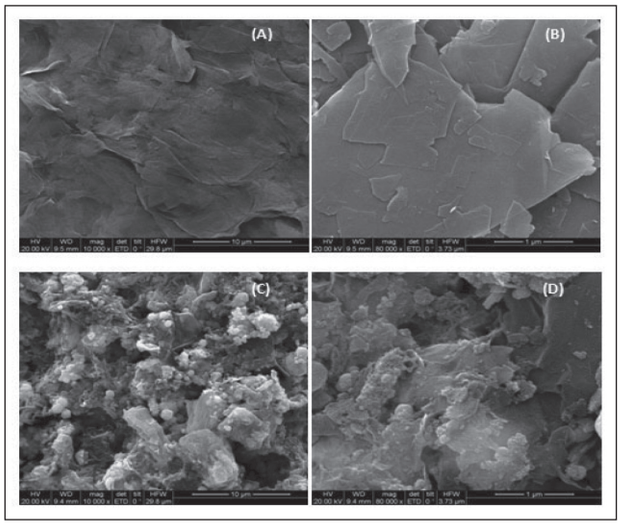

Fig. 1: SEM images of GO (A, B) and GO-Fe_3O_4 (C, D)

58.62° (511), and 63.75° (440), respectively (see Fig. 3b), which are well-matched with standard Fe_3O_4 (JCPDS. Card NO.19-0629). It can be found out that the diffraction peak of GO at 11.80° (001) did not appeared in the peaks of GO-Fe_3O_4, which may be attributed to the structural distortion of GO in GO-Fe_3O_4 system (Madadrang et al. 2012).

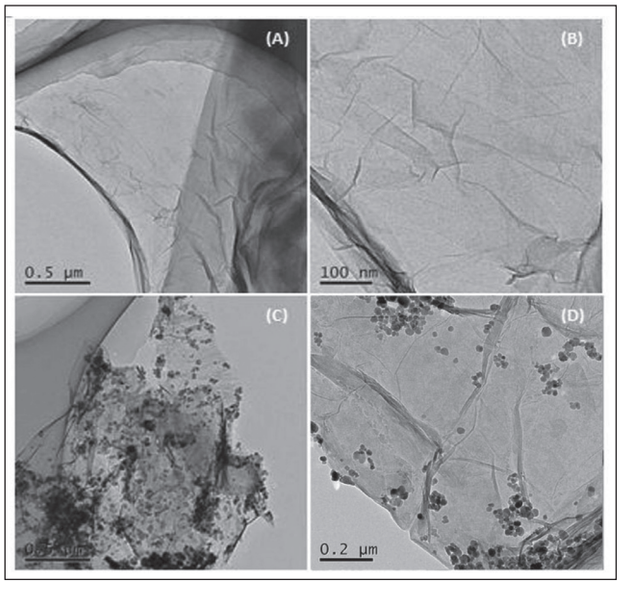

Fig. 2: TEM images of GO (A, B) and GO-Fe3O4 (C, D)

FT-IR analysis was carried out in the 400–4000 cm^{-1} range to investigate the chemical bonding of GO, Fe_3O_4 and GO-Fe_3O_4 hybrid, and the findings are presented in Fig. 3(c). From this Fig., the strong absorption peak of GO-Fe_3O_4 at 3425 cm^{-1} was the stretching vibration peak of –OH, while the peak at 1632 cm^{-1} could be attributed to aromatic C=C vibrations of the skeletal vibrations for unoxidized graphitic domains(Ouyang et al. 2015). The new peak at 563 cm^{-1} corresponded to the stretching vibration of the Fe-O bond, indicating the formation of Fe-O bonds between GO and Fe_3O_4. The formation of GO-Fe_3O_4 was confirmed by FT-IR spectra.

2.2. *Magnetism of GO-Fe_3O_4*

A vibrating sample magnetometer (VSM) was used for characterizing the magnetic properties of samples. From Fig. 3(d), the measured saturation magnetization value of Fe_3O_4 and GO-Fe_3O_4 was 75.17 and 58.42 emu/g respectively. The result showed that GO-Fe_3O_4 was still superparamagnetic, and the reduction of the saturation magnetization value of 6.75 emu/g for GO-Fe_3O_4 attributed to the existence of the GO. Furthermore, the insert image exhibited a dispersion and quick separation process of the GO-Fe_3O_4. It is easy to see that the GO-Fe_3O_4 is well dispersed in water with the absence of an external magnetic field and can be easily separated in the presence of an external magnetic field.

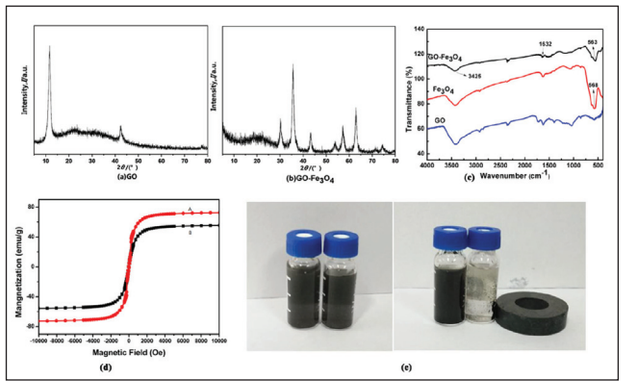

Fig. 3: XRD patterns of GO (a), GO-Fe_3O_4 (b), FT-IR spectra of GO, Fe_3O_4 and GO-Fe_3O_4 (c), hysteresis curve (M-H curve) of GO (A) and GO/Fe_3O_4 (B)at room temperature (d), changes in the distribution of GO-Fe_3O_4 under the external magnetic field (e).

2.3. *TMZ loaded on GO-Fe_3O_4*

The maximum drug loading capacity is an important factor for evaluating the therapeutic potential of a carrier. In this study, TMZ was loaded on GO-Fe_3O_4 surface through hydrogen bonding and intermolecular adsorption between GO and TMZ. As shown in Fig. 4(a), initially the drug loading capacity of GO-Fe_3O_4 increased sharply with the concentration of TMZ increasing till the TMZ concentration reached to 0.7 mg/ml; further increase the TMZ concentration reached to 1.5 mg/ml, drug loading capacity increased slightly; loading capacity dropped when TMZ concentration was greater than 1.5 mg/ml. The maximum drug loading was 6.47±0.08 mg/mg at the concentration of TMZ at 1.5 mg/ml. The drug loading efficiency of GO-Fe_3O_4 was calculated according to TMZ standard curve, and the loading efficiency at peak drug loading was 43.10±0.11 %. The result showed the drug loading efficiency of GO-Fe_3O_4 (ranged from 40% to 90%) was higher than that of other drug carriers, for example, the loading capacity of liposomes was usually below 40%. Therefore, GO-Fe_3O_4 is an excellent nanocarrier for delivery of TMZ-targeted formulations.

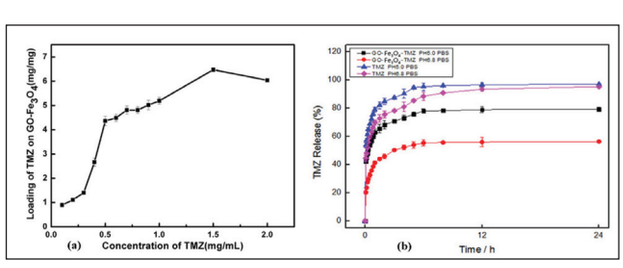

Fig. 4: Drug loading capacity of GO-Fe_3O_4 carrier at different concentrations of TMZ (n=6) (a), *In vitro* release profiles of TMZ at different pH (5.0 and 6.8) at 37 °C (b).

2.4. *TMZ released from GO-Fe_3O_4-TMZ*

Given the high loading capacity of GO-Fe_3O_4 composite toward TMZ, it may be used as a potential drug carrier. However, drug release behavior from a carrier are affected by many external

Table: In vitro release model fitting of TMZ and GO-FA-TMZ

	Models	Regression equations	R^2
TMZ	zero-order kinetics	Q=3.3977t + 69.151	0.6433
	first-order kinetics	Q=85.8058*(1-exp(-5.93086*t))	0.5272
	Higuchi	Q=14.0077*(t^(1/2))+59.02836	0.8373
	Ritger-Peppas	Q=75.5*(t^0.12)	0.9658
	Weibull	Q=99.006*(1-exp(-(2.5033*(t+0.1296))^0.4065))	0.9948
GO/Fe_3O_4-TMZ	zero-order kinetics	Q=2.9868t+ 54.602	0.6410
	first-order kinetics	Q=69.57*(1-exp(-5.189*t))	0.5375
	Higuchi	Q=12.2331*(t^(1/2))+45.8177	0.8555
	Ritger-Peppas	Q=60.1889*(t^0.13362)	0.9714
	Weibull	Q=80.3386-49.2799*exp(-(0.9231*t)^0.5631)	0.9956

factors, such as pH values, the interactions between the drug and carrier, and their physical and chemical properties. To clarify the release behavior of TMZ from GO-Fe_3O_4-TMZ composites, the release rates of TMZ under different conditions of 5.0 and 6.8 at 37 °C were investigated in the following experiments. As shown in Fig. 4(b), the TMZ released slowly from GO-Fe_3O_4-TMZ composites and a slightly acidic condition could be suitable for TMZ releases. The cumulative amount of TMZ from GO-Fe_3O_4-TMZ composites reached 74.86% at 8 h under the weak acid condition of pH 5.0. However, a fewer cumulative amount of 57.24% at 8 h was observed in a neutral condition of pH 6.8. As described in the literature, the hydrogen-bonding interaction between TMZ and GO-Fe_3O_4 is more firmly under neutral than under acidic conditions, resulting in an inefficient release (Pourjavadi et al. 2015; Kassaee et al. 2011). As the extracellular tissues of tumors, intracellular lysosomes and endosomes are acidic, this sensitive property of slightly acid for GO-Fe_3O_4-TMZ can be beneficial for the drug release in the acidic tumor microenvironment.

In addition, the release behavior of TMZ from GO-Fe_3O_4-TMZ composites was studied by fitting experimental data to five different kinetic models (zero-order kinetics, first-order kinetics, Higuchi, Ritger-Peppas, and Weibull models) (Maity and Sa 2016; Sang et al. 2018). The fitting equations are displayed in the Table, which shows the relation coefficient (R^2) of five kinds of release curves. Compared with other equations, the Weibull model has the largest R^2 value, thus the best-fit equation was the Weibull equation. The result of this study was consistent with the theory.

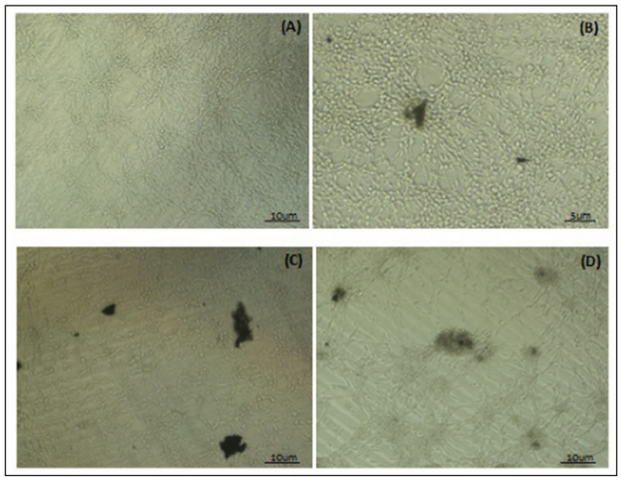

Fig. 5: Morphology of C6 cells cultured with GO-Fe_3O_4 after different times (A: 0 h, B: 24 h, C: 48 h, D: 72 h).

2.5. Cytotoxicity experiments

To evaluate the cytotoxicity of GO-Fe_3O_4-TMZ to tumor cells, MTT assays were performed and rat glioma C6 cells were selected. First, the cytotoxicity of GO-Fe_3O_4 was tested and results were shown in Fig. 5. The morphology of C6 cell cultured with GO-Fe_3O_4 for different periods (24 h, 48 h, and 72 h) was pretty much the same as initial morphology of C6 cell, no obvious changes were identified even at a higher concentration of 80 μg/ml. Furthermore, results of cell viability experiments showed that the cell viability of C6 cells was more than 91% after cultured with GO-Fe_3O_4 at the concentration of 120 μg/ml for 72 h (see Fig. 6(a)). All above results indicated the non-cytotoxic property of GO-Fe_3O_4.

The cytotoxicity test result of GO-Fe_3O_4-TMZ is shown in Fig. 6(b). Clearly, the inhibition rate increased with the increase in concentration of GO-Fe_3O_4-TMZ and culture time, which was consistent with the change rule of TMZ inhibition rate (Fig. 6(c)). After C6 cells were cultured using GO-Fe_3O_4-TMZ under the concentration of 600 μg/ml for 72 h, the cell inhibition rate of GO-Fe_3O_4-TMZ reached to 89.37 %. That is to say, GO-Fe_3O_4-TMZ had a better inhibitory effect on the proliferation of rat glioma C6 cells, and presented the time-and dose-dependent characteristic. In addition, it can be found that inhibition rate of GO-Fe_3O_4-TMZ was higher that of TMZ in the same condition after 48 h (Fig. 6(d)), which may be attributed to the sustained-release property of GO-Fe_3O_4-TMZ.

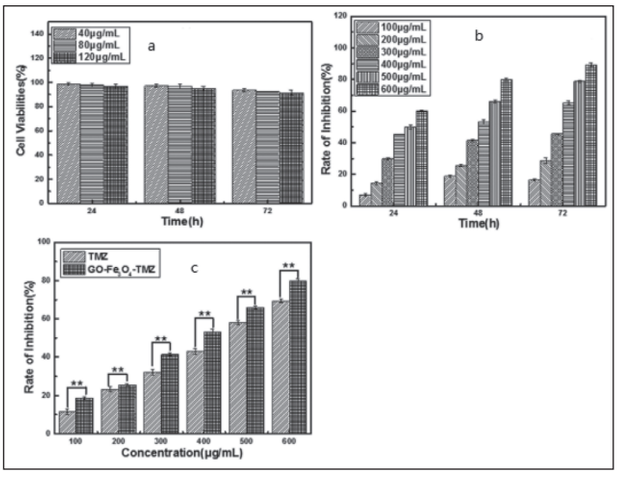

Fig. 6: MTT assay for the GO/Fe_3O_4 (a), GO/Fe_3O_4-TMZ (b) and comparison of TMZ and GO-Fe_3O_4-TMZ (c) The results in Fig. 6(c) has subtracted the effect of cells by themselves or cells with GO-Fe_3O_4. Statistical testing was performed using two-way ANOVA. (**$P < 0.01$)

In summary, the objective of this study was accomplished by designing GO-Fe_3O_4 nanoparticles of TMZ. With combining of GO sheets with Fe_3O_4 nanoparticles, the GO/Fe_3O_4 showed multi-

functional characterization of GO sheets and magnetic properties of Fe_3O_4. The GO-Fe_3O_4 displayed a strong magnetic property and could be controlled by an external magnetic field. Moreover, the GO-Fe_3O_4 has a high drug loading capacity for TMZ. According to the experimental results, GO-Fe_3O_4-TMZ showed good biocompatibility and pH-dependent release behavior. Thus, the developed GO/Fe_3O_4-TMZ nanoparticles can be used for the potential treatment of brain tumors.

3. Experimental

3.1. Materials

TMZ was purchased from Biolang Biotechnology Co., Ltd. (Shanghai, China). GO was obtained from Fenghua Material Development Co., Ltd. (Hubei, China). Ham's F12K medium was obtained from GIBCO (Grand Island, NY, USA). Ferric chloride hexahydrate ($FeCl_3{\cdot}6H_2O$), ferrous chloride tetrahydrate ($FeCl_2{\cdot}4H_2O$), dimethyl sulfoxide (DMSO) and ammonia ($NH_3{\cdot}H_2O$) used in this study were of analytical grade.

3.2. Synthesis of GO-Fe_3O_4

GO-Fe_3O_4 nanocomposites were synthesized by the co-precipitation method according to the literature with slight modification (Huang et al. 2017). In brief, $FeCl_3$ solution and $FeCl_2$ solution (molar ratio of Fe^{2+}:Fe^{3+}=1:2) were slowly added into graphene oxide dispersion (1 mg/mL) under nitrogen for 1 h. Then, an ammonia solution was injected into the solution and the reaction was continued for 4 h at 80 °C. Afterwards, the obtained black precipitate was collected and washed with distilled water three times to remove reactants. The GO-Fe_3O_4 nanocomposites were dried in a vacuum oven at 40 °C before use.

3.3. Characterization of GO-Fe_3O_4

The morphology and microstructure of GO-Fe_3O_4 were observed through a S-4800 scanning electron microscope (SEM, Hitachi, Japan) operating at 20.00 kV and Tecnai G220 transmission electron microscope (TEM, FEI, USA). FT-IR spectra were recorded on a 650-Fourier Transform Infrared Spectrometer (Tianjin GangDong Sci. & Tech. Development Co., Ltd., China) with the wavenumber ranged from 400 cm^{-1} to 4000 cm^{-1}. X-ray diffraction (XRD) was performed by the 7000-X-ray diffractometer (Shimadzu, Japan) in a scanning range of 5 ° to 80 ° with the tube voltage of 40 KV and current of 30 mA. The hysteresis loop of GO-Fe_3O_4 was measured by the MPMS DynaCool hysteresis loop instrument (Quantum Design, USA) with the scanning range from -20KOe to 20KOe.

3.4. TMZ loading and release of GO-Fe_3O_4-TMZ

TMZ at different concentrations were mixed with GO-Fe_3O_4 (the concentration of 0.1 mg/mL) (1:1) in a shaker at room temperature for 24 h. The magnetic complex of GO-Fe_3O_4 loaded with TMZ (GO-Fe_3O_4-TMZ) was separated by centrifugation at 10,000 rpm for 0.5 h. The clear supernatant at the top was collected, and the concentration of TMZ in the supernatant was measured by HPLC. The loading capacity of TMZ in GO-Fe_3O_4 was calculated based on the following formula:

$$\text{Drug loading capacity} = (W_{\text{initial dose}} - W_{\text{residual dose in solution}})/W_{\text{carrier}} \quad (1)$$

where $W_{\text{initial dose}}$ is the initial weight of TMZ before loading, $W_{\text{residual dose in solution}}$ is the weight of residual TMZ in solution after loading, and W_{carrier} is the weight of GO-Fe_3O_4.

The release behavior of TMZ from GO-Fe_3O_4 was investigated by dynamic membrane dialysis. The drug-loaded GO-Fe_3O_4 was dispersed in PBS with pH of 5.0 and 6.8, respectively. Samples of 3 ml of eluate were taken after certain time interval (0.083, 0.167, 0.25, 0.33, 0.5, 0.67, 0.83, 1, 1.5, 2, 3, 4, 5, 6, 8, 12, 24 h) for the determination of dissolution rate, then the same volume of PBS buffer was added. The concentration of TMZ was measured by HPLC, and the cumulative release rate was calculated based on the following formula:

$$W = (C_t V + \sum C_t V_t)/(C_0 V_0 - C_1)$$

where W is the cumulative release rate, V is the volume of phosphate buffer, C_0 is the initial TMZ concentration, V_0 is the initial TMZ volume, C_1 is the TMZ concentration in supernatant after centrifugation, V_1 is the volume of supernatant by centrifugation after loading, C_t is the concentration of TMZ in buffer solution, and V_t represents the volume of the buffer solution taken out at this time.

In this experiment, five different kinetic models (zero-order kinetics, first-order kinetics, Higuchi, Ritger-Peppas and Weibull models) were adopted to explain the release behavior of TMZ in GO-Fe_3O_4-TMZ system, where the optimum kinetic model was selected based on the values of R^2.

3.5. Cell culture and cytotoxicity experiments

In order to investigate the targeted and therapeutic effects of GO-Fe_3O_4-TMZ to tumor cells, rat glioma C6 cells were selected. The rat glioma C6 cells were seeded in 96-well plates and cultured with GO-Fe_3O_4-TMZ in the dark at 37 °C under the humidified atmosphere (5 % CO_2) for different time intervals (24 h, 48 h and 72 h). Meanwhile, cells also cultured with GO-Fe_3O_4 as control group. The morphology of rat C6 glioma cells was observed by microscope.

In a cytotoxicity experiment, rat glioma C6 cells were seeded in a 96-well plate with the density of 4×10^4 cells per well. After 24 h, the medium was discarded, and the cells were cultured with different concentrated GO-Fe_3O_4-TMZ and GO-Fe_3O_4 (0 mg/l, 100 mg/l, 200 mg/l, 300 mg/l, 400 mg/l, 600 mg/l, 800 mg/l), respectively. After reacted for 4 h, MTT solution (0.5 %, 10 µl) was added into each well, and the cells was further cultured for 4 h. At the end of the incubation, DMSO (100 µl) was added into each well and dissolved for 10 min. The optical density (OD) was measured by using the micro-plate reader (Multiskan FC, Thermo Electron Co., America) at the wavelength of 490 nm. The rat glioma C6 cell line was used to evaluate the drug delivery and imaging capability of GO-Fe_3O_4-TMZ.

3.6. Magnetic targeting of GO-Fe_3O_4-TMZ in vitro

In this section, the C6 cells were cultured in the 96-well culture plate for 48 h with GO-Fe_3O_4-TMZ as the medium. Meanwhile, a magnetic field was set on one side. The distribution of GO-Fe_3O_4-TMZ and the growth status of the cells were observed.

3.7. Statistical analysis

All the experiments were performed in duplicates and the results are expressed as mean±standard deviation (SD). Repeated measured two-way ANOVA followed by the Bonferroni post-hoc test was used to statistically compare data.

Acknowledgements: This study was supported by Educational Department of Hebei Provincial (No. QN2015221), Science and Technology and Earthquake Bureau of Zhangjiakou (No. 1811019A), and Foundation of Hebei North University (No. YB2018019).

Conflicts of interest: None declared.

References

Bédard MF, Braun D, Sukhorukov GB, Skirtach AG (2008) Toward self-assembly of nanoparticles on polymeric microshells: near-IR release and permeability. Acs Nano 2: 1807-1816.

Chai PV, Mohammad A, Teow YH, Mahmoudi E (2017) Evaluation of Iron oxide decorated on graphene oxide (FE3O4/GO) nanohybrid incorporated in PSF membrane at different molar ratios for Congo red rejection. Jurnal Teknologi 79: 73-81.

Cole AJ, Yang VC, David AE (2011) Cancer theranostics: the rise of targeted magnetic nanoparticles. Trends Biotechnol 29: 323-332.

Deng H, Li X, Peng Q, Wang X, Li, Y (2005) Monodisperse magnetic single-crystal ferrite microspheres. Angew Chem 44: 2782-2785.

Gio L, Shi H, Wu H, Zhang Y, Wang X, Wu D, Aa L, Yang S (2016) Prostate cancer targeted multifunctionalized graphene oxide for magnetic resonance imaging and drug delivery. Carbon 107: 87-99.

Huang YS, Lu YJ, Chen JP (2017) Magnetic graphene oxide as a carrier for targeted delivery of chemotherapy drugs in cancer therapy. J Magnet Magnet Mat 427: 34-40.

Kassaee MZ, Motamedi E, Majdi M (2011) Magnetic Fe3O4-graphene oxide/polystyrene: Fabrication and characterization of a promising nanocomposite. Chem Engin J 172: 540-549.

Li J, Pei Q, Wang R, Zhou Y, Zhang Z, Cao Q, Wang D, Mi W, Du Y (2018) Enhanced photocatalytic performance through magnetic field boosting carrier transport. ACS Nano 12: 3351-3359.

Li J, Zhang S, Chen C, Zhao G, Yang X, Li J, Wang X (2012) Removal of Cu(II) and fulvic acid by graphene oxide nanosheets decorated with Fe_3O_4 nanoparticles. ACS Appl Mater Interfaces 4: 4991-5000.

Madadrang CJ, Kim HY, Gao G, Wang N, Zhu J, , Feng H, Gorring M, Kasner ML, Hou S (2012) Adsorption behavior of EDTA-graphene oxide for Pb (II) removal. ACS Appl Mater Interfaces, 4, 1186-93.

Maity S, Sa B (2016) Compression-coated tablet for colon targeting: impact of coating and core materials on drug release. AAPS PharmSciTech 17: 504-515.

Noble PF, Cayre OJ, Alargova RG, Velev OD, Paunov VN (2004) Fabrication of "hairy" colloidosomes with shells of polymeric microrods. J Am Chem Soc 126: 8092-8093.

Nordling-David MM, Yaffe R, Guez D, Meirow H, Last D, Grad E, Salomon S, Sharabi S, Levi-Kalisman Y, Mardor Y (2017) Liposomal temozolomide drug delivery using convection enhanced delivery. J Control Release 261: 138-146.

Ouyang K, Zhu C, Zhao Y, Wang L, Xie S, Wang Q (2015) Adsorption mechanism of magnetically separable Fe 3 O 4 /graphene oxide hybrids. Appl Surface Sci 355: 562-569.

Pankhurst QA, Connolly J, Jones SK, Dobson J (2003) Applications of magnetic nanoparticles in biomedicine. J Phys D 36: R167.

Pourjavadi A, Shakerpoor A, Tahrani ZM, Bumajdad A (2015) Magnetic graphene oxide mesoporous silica hybrid nanoparticles with dendritic pH sensitive moieties coated by PEGylated alginate-co-poly (acrylic acid) for targeted and controlled drug delivery purposes. J Polymer Res 22: 156.

Prabhu S, Goda JS, Mutalik A, Mohanty BS, Chaudhari P, Rai S, Udupa N, Rao BSS (2017) A polymeric temozolomide nanocomposite against orthotopic glioblastoma xenograft: tumor-specific homing directed by nestin. Nanoscale 9: 10919.

Pramanik N, Ranganathan S, Rao S, Suneet K, Jain S, Rangarajan S, Jhunjhunwala S (2019) A composite of hyaluronic acid-modified graphene oxide and iron oxide nanoparticles for targeted drug delivery and magnetothermal therapy. ACS Omega 4: 9284-9293.

Sang G, Bardajee GR, Mirshokraie A, Didehban K (2018) A thermo/pH/magnetic-responsive nanogel based on sodium alginate by modifying magnetic graphene oxide: Preparation, characterization, and drug delivery. Iran Polymer J 27: 137-144.

Schleich N, Po C, Jacobs D, Ucakar B, Gallez B, Danhier F, Preat V (2014) Comparison of active, passive and magnetic targeting to tumors of multifunctional paclitaxel/SPIO-loaded nanoparticles for tumor imaging and therapy. J Control Release 194: 82-91.

Wang Y, Li Z, Wang J, Li J, Lin Y (2011) Graphene and graphene oxide: biofunctionalization and applications in biotechnology. Trends Biotechnol 29: 205-212.

Yang H, Bremser DH, Tao L, Li H, Hu J, Zhu L (2016) Carboxymethyl chitosan-mediated synthesis of hyaluronic acid-targeted graphene oxide for cancer drug delivery. Carbohydr Polym 135: 72-78.

Yue H, Wie W, Yue Z, Wang B, Luo N, Gao Y, Ma D, MA G, Su Z (2012) The role of the lateral dimension of graphene oxide in the regulation of cellular responses. Biomaterials 33: 4013-4021.